# Assessing the present-day terrestrial carbon cycle from a variety of data-driven carbon cycle models and a process-based phenology model

M. Leonard[1,2], L. Bruhwiler[1], A. R. Jacobson[1,2], A. Kaushik[1,2], B. Rastogi[1,2], Baker[3], K. Haynes[3], S. Denning[3], A. Subramanian[4]

[1]NOAA Earth System Research Laboratory, Global Monitoring Laboratory, Boulder, CO, United States
[2]Cooperative Institute for Research in Environmental Sciences, University of Colorado, Boulder, CO, United States
[3]Department of Atmospheric Science, Colorado State University, Fort Collins, CO, United States
[4]Department of Atmospheric and Oceanic Sciences, University of Colorado, Boulder, CO, United States
Corresponding author: Mark Leonard (mark.leonard@noaa.gov)

## Key Findings:

- Top-down and bottom-up models agree each region has an annual terrestrial carbon sink from 2000-2017.
- Inversion models suggest the 2000-2017 increase in high-latitude CO2 seasonal amplitude is a result of increased respiration from Oct-Dec.
- Models do not show a statistically significant NEE, RE, or GPP trend at any TransCom regions from 2000-2017.

## Abstract

Carbon cycle-climate feedback involving terrestrial carbon exchanges with the atmosphere is a major contributor to uncertainties in climate projections. To provide a comprehensive perspective of the terrestrial carbon cycle and potential changes that could influence the climate system, we combine and analyze various "bottom-up" terrestrial process-based models and "top-down" atmospheric inverse models between 2000-2017. All models and data products estimate the global terrestrial surface to be an annual net sink of $CO_2$, yet none produces statistically significant carbon flux trends on continental scales. Inverse models suggest that the $CO_2$ seasonal cycle amplitude enhancement at boreal latitudes results from increased carbon respiration during early winter (Oct-Dec) that exceeds uptake rates during summer months (Jun-Aug). As more data becomes available over time, these models are useful tools for evaluating and narrowing the uncertainties associated with the process representation of the terrestrial carbon cycle.

## 1 Introduction

Earth System Models (ESMs) participating in the 5th Coupled Model Intercomparison Project (CMIP5) (Taylor et al., 2012) have shown that large variability in twenty-first century $CO_2$ projections are mainly due to uncertainties in terrestrial carbon cycle processes (Friedlingstein et al., 2013). These terrestrial carbon cycle uncertainties are found to be mostly due to differences in how ESMs represent their own physical climate system and global biosphere modeling (Lovenduski and Bonan, 2017). In this study, we focus on a better understanding of the global biospheric structure.

Increased observational coverage over 50 years has provided important insights into how carbon is exchanged between the biosphere and the atmosphere around the globe. However, it is still uncertain how it exchanges of carbon between the atmosphere and the biosphere will respond to increasing $CO_2$ emissions. Global biospheric carbon fluxes can be estimated using a "bottom-up" or "top-down" approach. A "bottom-up" scaling approach involves extrapolating measurements of carbon variability and processes from very local scales (of about 100 $m^2$) to larger regional scales using ancillary datasets (e.g., vegetation and soil maps, environmental data). Terrestrial biosphere models (TBM)s can also be considered a bottom-up approach because they simulate carbon exchanges in detail globally. Important locally-scaled measurements include surface-based biomass inventory and a global multidecadal FLUXNET network of hundreds of site-level eddy covariance flux towers with the most significant observational coverage in temperate North America, Europe, and Japan. This approach provides local-scale carbon cycle processes and variability, but its disadvantage is not knowing how representative these measurements are over a broader region. TBMs are often accompanied by space-based observing systems that expand observational coverage in areas of limited surface measurements, albeit with validation challenges. Multidecadal remote sensing records have monitored "greening" trends at high latitudes, ecosystem disturbances, and land-use changes that alter the carbon sources and sinks over short- and long-time scales. Taken together, bottom-up TBMs are capable of providing local-scale carbon cycle processes and variability.

The "top-down" approach we consider in this study is inverse modeling, which employs numerical optimization techniques to estimate carbon sources and sinks using spatial and temporal variability from atmospheric $CO_2$ observations. The advantage of this approach is that it provides an independent estimate of carbon fluxes over a larger region while capturing the observed variability from globally distributed atmospheric CO2 observations. The disadvantage is that it provides little information about underlying processes that cause net carbon sources and sinks at smaller scales. In essence, inverse modeling can only infer a cause (surface carbon sources and sinks) to an observed effect (actual changes in atmospheric $CO_2$ concentration). As more observations are collected over time, inverse modeling can provide an estimate of how and where regional carbon fluxes may be changing.

Bottom-up and top-down approaches often produce conflicting results. For example, at high northern latitudes, atmospheric $CO_2$ observations suggest increased carbon uptake by the terrestrial biosphere and "greening" trends detected by satellite-remote sensing may indicate increased carbon uptake by $CO_2$ fertilization or warming at high northern latitudes (Mao et al., 2016). However, the FLUXNET network does not appear to show uptake due to $CO_2$ fertilization and instead shows increased carbon loss from plants and soils sensitive to warming temperatures (Kaushik et al., 2020). In this study we combine these complementary "bottom-up" and "top-down" modeling approaches, also known as a multiple-constraint approach, to better quantify the global terrestrial carbon sources and sinks over the recent past.

We examine three different types of TBMs: the Carnegie-Ames-Stanford Approach model (CASA; Potter et al., 1993), the SiBCASA model, which combines biogeochemistry from CASA with biophysical processes from the Simple Biosphere model (Schaefer et al., 2008), and a newly developed predictive phenology strategy implemented in the Simple Biosphere Model, version 4.2 (SiB4; Haynes et al., 2019a; 2019b). The first two methods to calculate global carbon fluxes are diagnostic because they depend on available satellite-based Normalized Difference Vegetation Index (NDVI) to track plant phenology, whereas the latter is prognostic and predicts phenology.

Another bottom-up approach used to understand the present-day land carbon cycle is upscaling in-situ site-level observations to estimate the global Net Ecosystem Exchange (NEE). The FLUXCOM data product upscales the global FLUXNET network to regional and global scales using machine learning methods that incorporate satellite remote sensing and meteorological data (Tramontana et al., 2016; Jung et al., 2020). Details are discussed in section 2.1.

For our “top-down” approach, we examine the posterior carbon flux estimates from the data assimilation (DA)/flux-inversion model CarbonTracker (Peters et al., 2007; Jacobson et al.,

2020) developed at the National Oceanic and Atmospheric Administration (NOAA) and the European version, CarbonTracker-Europe (van der Laan-Luijkx et al., 2017). These posterior fluxes are estimated using the TBMs SiBCASA and CASA as prior flux estimates that are then optimally adjusted to match the spatiotemporal variability of observed atmospheric $CO_2$ using an atmospheric chemical transport model.

In this study we will examine whether we can learn more about how changes in the terrestrial carbon cycle may have led to the observed increase in $CO_2$ amplitude at high latitudes (Graven et al., 2013) by using both process-based and "multiple constraint" models and evaluating their consistency. Graven et al., (2013) examined the seasonal amplitude of $CO_2$ observed at Barrow Atmospheric Baseline Observatory (BRW), Alaska and found increases of 50% over 50 years and smaller increases of 25% at Mauna Loa Observatory (MLO), Hawaii. They concluded that carbon uptake is more rapidly increasing at high latitudes (45°-90°N) than at lower latitudes (10°-25°N). This study implies ecological changes in boreal forests such as increased stand area and biomass (Pan et al., 2011) or northward tree expansion due to warming (Elmendorf et al., 2012). These changes are not accounted for in many CMIP5 models, resulting in underestimated changes in NEE over the past 50 years and uncertainty about whether future projections are accurate. Later studies suggested the intensification of agriculture in the northern hemisphere over the past several decades contribute up to a quarter to the observed seasonal amplitude increase at high latitudes (Zeng et al., 2014; Gray et al., 2014). More recent studies used top-down studies to suggest the Siberian and temperate ecosystems have been a main contributor to the observed amplitude increase at BRW (Lin et al., 2020).

The main objectives of this study are the following: (1) determine whether process-based and "multiple constraint" models are consistent in terms of terrestrial carbon flux strength and seasonal variability on global and regional scales from 2000-2017; and (2) quantify how both these fluxes and its seasonal variability may have changed over this time period.

## 2 Data and Methods

### 2.1 Model Descriptions

This section briefly describes the carbon cycle models used in this study, beginning with the TBMs (CASA-GFED and SiBCASA) used as first-guess estimates for two versions of the atmospheric inversion model CarbonTracker. Thereafter, we briefly describe the similarities and differences of the. Lastly, we describe the FLUXCOM product and the new predictive-phenology-based TBM SiB4.

### 2.1.1 Prior Flux Fields: CASA and SiBCASA

The Carnegie-Ames-Stanford Approach (CASA; Potter et al., 1993) terrestrial carbon cycle model uses satellite-derived NDVI, a simple light efficiency model and meteorological drivers to simulate monthly net primary production (NPP). Both CT2019 prior fluxes are driven using Advanced Very High-Resolution Radiometer NDVI. Calculating NPP requires an assumption that NPP is a constant fraction of the GPP and autotrophic respiration is the same size as NPP, but opposite sign for all ecosystems and geographical areas. CASA estimates heterotrophic respiration (RH) of $CO_2$ using a biomass pool structure with first-order equations. CASA NPP and RH are combined to simulate monthly NEE at a global 1°x 1° resolution.

SiBCASA is a hybrid of the Simple Biosphere Model, Version 2.5 (SiB2.5), and the CASA model (Schaefer et al., 2008). SiB2.5 is a biophysical model that estimates land-surface carbon fluxes at 10-20 minute resolution with global 1°x 1° degree resolution (Sellers et al., 1986, 1996a, 1996b; Denning et al., 1996). It uses biophysical processes to calculate variables such as temperature and moisture content at canopy tops and soil depths. SiB2.5 carbon uptake by gross primary productivity (GPP) is determined using enzyme kinetics (Farquhar et al., 1980) and stomatal physiology (Collatz et al., 1991; 1992) at a leaf level. These calculations are then scaled to the entire canopy using Photosynthetically Active Radiation (fPAR), Leaf Area Index (LAI), and vegetation cover fraction from Global Inventory Monitoring and Modeling System (GIMMS) NDVI data set, version g (Tucker et al., 2005). SiB2.5 GPP and ecosystem respiration (RE) is combined with CASA RH to provide global estimates of autotrophic respiration and non-fire net ecosystem exchange (NEE).

### 2.1.2 CarbonTracker CT2019B

NOAA's CarbonTracker is an atmospheric $CO_2$ modeling system that estimates surface fluxes that are in optimal agreement with available atmospheric $CO_2$ measurements. CarbonTracker is updated on a quasi-annual basis, and we use results from the latest version CT2019B (Jacobson et al., 2020). CT2019B simulates atmospheric transport using ERA-interim analyzed winds (Dee et al., 2011) within the TM5 atmospheric transport model (Krol et al., 2005) running at a global 3° longitude by 2° latitude resolution with a nested regional grid of 1°x 1° degree over North America.

The CT2019B estimation scheme requires first-guess, or prior, surface $CO_2$ flux estimates. This serves both to initialize the optimization scheme and to constrain flux estimates in locations with sparse observational information. To mitigate the sensitivity to prior fluxes, CT2019B conducts independent inversions using unique combinations of multiple prior flux estimates: two versions of the CASA model, two data-constrained models of air-sea $CO_2$ exchange, and two gridded estimates of fossil-fuel emissions. A description for these flux estimates can be found in sections 4 and 5 of Jacobson et al., (2020).

Posterior fluxes from these independent inversions are averaged to produce the final CT2019B flux estimate. CarbonTracker finds optimal surface fluxes by estimating a set of scaling factors that multiply net surface $CO_2$ exchange from the prior models. These scaling factors are estimated on a weekly basis, and over 239 ecoregions (i.e., 11 terrestrial Transcom regions contain a maximum of 19 ecoregion types) spanning the globe.

CT2019B assimilated more than 4.1 million measurements of atmospheric $CO_2$ mole fraction between 2000 and 2018. These measurements were collected from surface flask sampling networks, towers, aircraft, and shipboard platforms from 55 international laboratories and are grouped into the Observational Package (ObsPack) GLOBALVIEWplus data product version 5.0 (Cooperative Global Atmospheric Data Integration Project, 2019).

The atmospheric $CO_2$ measurements cover the entire globe but are not distributed uniformly. North America and Europe have a relatively high density of observations, but large regions of the tropics and Southern Hemisphere are sparsely observed. For use in inversions, each assimilated $CO_2$ measurement is assigned a model-data mismatch (MDM) error term, which expresses the statistical extent to which the model is expected to deviate from the measurement. In CT2019B, this MDM varies by site, season, local time of day, and altitude above the land surface. Temporal and spatial gaps in observational coverage can lead to errors in estimated surface fluxes, including the tendency of the model to stay close to a given prior flux estimate.

CT2019B uses two versions of the CASA model runs as prior flux estimates: The Global Fire Emissions Database project version 4 (GFEDv4.1s) and GFED used with the National Aeronautic and Space Administration (NASA's) Carbon Monitoring System (CMS). Both CASA model runs are driven by Advanced Very High-Resolution Radiometer (AVHRR) NDVI data.

By using multiple terrestrial priors, CT2019B mitigates potential prior biases that may propagate into the posterior flux product, though this assumes both priors do not have the same biases. To resolve diurnal and synoptic variability, CT2019B monthly priors with a 1°x 1° spatial resolution are temporally downscaled using a variant of the scheme introduced by Olsen and Randerson (2004) to simulate 3-hourly NEE of $CO_2$. This modified scheme avoids abrupt month-to-month changes in downscaled fluxes using a smoothing scheme introduced by Rasmussen (1991). Complete documentation, access to data products, and a detailed assessment of CT2019B performance are available at http://carbontracker.noaa.gov.

### 2.1.3 CarbonTracker-Europe CTE2018

We use the latest release of CarbonTracker Europe (hereafter "CTE2018") (van der Laan-Luijkx et al., 2017). CTE2018 uses a different set of first-guess prior surface $CO_2$ flux estimates and a different version of $CO_2$ data (as detailed below). Both inverse models use the ocean inversion flux (OIF) scheme to provide prior estimates of air-sea $CO_2$ flux (Jacobson et al., 2007), and CT2019B additionally uses an updated version of the Takahashi et al. (2009) $pCO_2$ climatology. CTE2018 uses a fossil fuel emission inventory developed by the CARBONES project by USTUTT/IER (see ier.uni-stuttgart.de) and CT2019B uses two emissions products called the "Miller" and "ODIAC" emissions datasets described in Jacobson et al., (2020). CTE2018 uses a single terrestrial prior flux field (as opposed to multiple priors used in CT2019B) derived from the SiBCASA model described in section 2.1.1. As SiBCASA simulates 1°x 1° resolution global fluxes on a 10-minute time resolution, temporal downscaling is not necessary as it is in CT2019B; albeit, a single prior flux estimate propagates potential biases into the posterior product. Both inversion models use TM5 at a global 3° longitude × 2° latitude resolution, and CTE2018 uses an additional nested regional grid at 1° × 1° resolution over Europe.

CT2019B assimilates these prior flux estimates with a more recent version of $CO_2$ data than CTE2018, but CTE2018 includes greater observational coverage over the Amazonia, Eurasia, and

Tropical Asia. Similar to CT2019B, each measurement is assigned an MDM mismatch error value, which varies by site, time, and location. Likewise, these measurements are not uniformly distributed over the globe. Temporal and spatial gaps in the observations lead to posterior fluxes closely resembling their prior flux estimates. Similar to CT2019B, a weekly set of unknown multiplicative scaling factors are applied to each of the land and ocean prior fluxes to be assimilated, but for a particular grid box of the global domain instead of the ecoregion regions used by CT2019B. Further information on CTE2018 documentation and available data products can be found at https://www.carbontracker.eu.

### 2.1.4 FLUXCOM

The FLUXCOM initiative generates a variety of global flux products by upscaling site-level eddy covariance observations of GPP and RE to produce non-fire NEE using different machine learning methods trained by different sets of satellite remote sensing and meteorological data (Jung et al., 2020; Tramontana et al., 2016). We use results from the remote sensing plus meteorological/climate forcing setup described by Jung et al. (2020) that is driven by meteorological forcing data from ERA-5 (C3S, 2017) and MODIS land products (collection 5; https://lpdaac.usgs.gov/) variables. The MODIS land products include temperature, land cover, and fPAR. The FLUXCOM dataset provides global flux estimates at a global 0.5° x 0.5° resolution with daily temporal resolution from 1979 to 2018, and are publicly available at Fluxcom.org.

Jung et al. (2020) found FLUXCOM NEE fluxes were consistent with the seasonal and inter-annual variability of atmospheric inversion models (including CTE2018 used in this study) across the northern hemisphere. However, a lack of consistent temporal and global coverage and systematic errors in FLUXNET data quality limit the use of FLUXCOM global flux products to extract natural signals (i.e. interannual variability and trends) and lead to unrealistic flux magnitudes e.g., a strong carbon sink in the tropics (Jung et al., 2020). As the FLUXNET network expands coverage in under-sampled regions, upscaling uncertainties can be expected to be reduced. Nevertheless, FLUXCOM global-scaled carbon flux products provide a useful bottom-up constraint on the global carbon cycle that can be readily compared with process-based or top-down models at regional and global scales.

### 2.1.5 SiB4

The Simple Biosphere Model version 4.2 (SiB4) is an environmentally responsive prognostic phenology model with dynamic carbon allocation and cascading carbon pools (Haynes et al., 2019; Baker et al., 2013; Lokupitiya et al., 2009; Schaefer et al., 2008; Sellers et al., 1996). SiB4 combines biogeochemical, biophysical, and phenological processes to predict vegetation and soil moisture, land surface energy and water budgets, and the terrestrial carbon cycle.

Rather than prescribing satellite-derived NDVI to track plant phenology, SiB4 fully simulates phenology by determining the above and belowground biomass, which impacts GPP and RE. At every 10-minute time-step predictor variables i.e. albedo, radiation, temperature, and soil moisture, as well as the resulting energy exchanges, moisture fluxes, carbon fluxes, and carbon pool transfers are computed at a global 0.5°x 0.5°degree resolution.

Similar to SiBCASA, photosynthesis depends directly on environmental factors (e.g. humidity, moisture, and temperature) and aboveground biomass, and carbon uptake, or assimilation, is determined using enzyme kinetics (Farquhar et al., 1980) and stomatal physiology (Collatz et al., 1991; 1992). Carbon outgassing through autotrophic and heterotrophic respiration (combined to form ecosystem respiration (RE)) depends on biomass growth and maintenance as well as moisture, temperature, and the carbon pools.

Carbon is transferred between carbon pools once daily as a function of assimilation rate, day length, moisture, temperature, and pool size. Once the pools are updated, the state of the carbon cycle, energy exchanges, moisture fluxes, and related predictor variables are revised, thus providing a self-consistent prognostic system.

SiB4 framework is designed to ensure an annual balance for global terrestrial carbon budget (NEE=0) because natural carbon uptake and release is largely balanced on global scales (Schimel et al., 1995). However, SiB4 is capable of producing unbalanced fluxes by incorporating additional sources and sinks (e.g. disturbances, dynamic vegetation, $CO_2$ fertilization, nutrient limitation, and regrowth). Yet, such external sources and sinks likely only offset the global annual balance by only a small percentage (Denning et al., 1996).

SiB4 has been evaluated globally against the FLUXNET network, satellite solar-induced fluorescence (SIF), and satellite-derived LAI and biomass (Smith et al., 2017; Haynes et al., 2019; Parazoo et al., 2020) and has been found to have improved predictions over grasslands (Haynes et al., 2019b).

## 2.2 Carbon Flux Analysis

### 2.2.1 Seasonal variability and annual total analysis

In this study, we determine whether terrestrial carbon models produce a net carbon source or sink to the atmosphere from 2000 to 2017. To create annual NEE (excluding fire emissions) for each model by calculating their global sum in units of PgC yr$^{-1}$. This process is repeated for 11 different land regions defined by the TransCom project (Gurney et al., 2002). Each region represents a continent-scale terrestrial area of broadly similar ecosystem types (Figure 1). Furthermore, they are used in the CT2019B data assimilation (DA) scheme as source regions for which estimates of land and ocean surface fluxes are produced. Following CT2019B's DA scheme, in which optimized fluxes from multiple inversions are averaged together to form a final posterior flux estimate, we average together terrestrial priors (i.e. CASA-GFEDv4.1s and CASA-CMS) to form a representative single prior flux estimate for CT2019B.

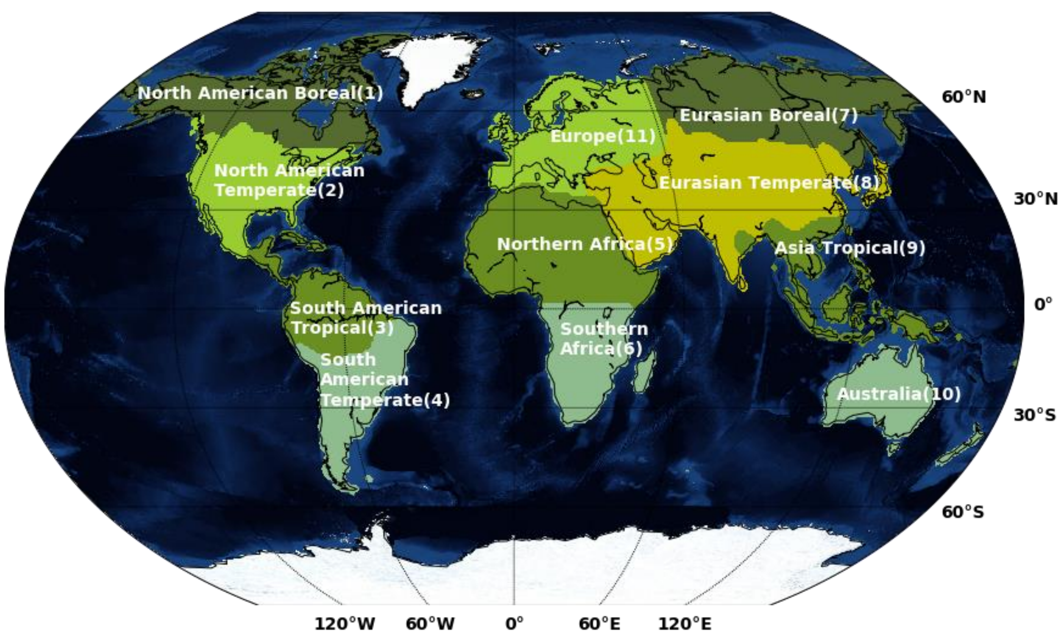


Figure 1. Terrestrial $CO_2$ flux regions of the TransCom inter-comparison project (Gurney et al., 2002).

To examine the structure of the terrestrial carbon seasonal cycle at regional scales, we produced monthly averaged fluxes from the models for 2000-2017. With monthly fluxes, we calculated the amplitude and phase of the seasonal cycle for RE and GPP for each model to gain additional information about the biospheric flux components that drive the terrestrial carbon cycle. For each region, monthly time series were averaged over 2000-2017 to produce a 12-month seasonal cycle. Seasonal cycles were compared among the models using a R-squared metric.

Likewise, we conduct a trend analysis to determine whether the model's terrestrial carbon cycle fluxes have changed over the recent past. Here we apply a linear least-squares regression to determine whether a model's net land fluxes detect any "statistically meaningful" trends (i.e. $r^2 \geq 0.65$ at $p \leq 0.05$) over the 18-year period using the criterion described in Bryhn & Dimbeg (2011). This process is repeated for GPP and RE on global and regional scales. We do not include SiB4 in the trend analysis as it assumes a long-term carbon balance and we are considering an 18-year period.

### 2.1.1 Boreal seasonal amplitude enhancement

Graven et al., (2013) concluded that increases in $CO_2$ amplitude from Barrow Atmospheric Baseline Observatory (BRW; see for more details https://www.esrl.noaa.gov/gmd/obop/brw/) between 1961-2011 are due to increased biogenic carbon uptake in northern latitude region (north of 45N). Our study assesses how well inverse models reproduce the $CO_2$ seasonal cycle at BRW and its increased seasonal amplitude. We calculate the seasonal amplitude trend of $CO_2$ using an average annual growth rate over the years 1972-2017 and 2000-2017 for both BRW observations and inversions.

Using inverse models, we examine how these seasonal $CO_2$ amplitude trends translate into annual NEE changes in the boreal region (north of 45˚N). For each model, we produce annual cycle NEE amplitudes, as well as a 3-month averaged NEE over months of peak carbon uptake from the atmosphere into the biosphere (i.e. June, July, and August) and early winter carbon release from the biosphere into the atmosphere (October, November, and December).

## 3 Results

### 3.1 Seasonal Cycle Analysis

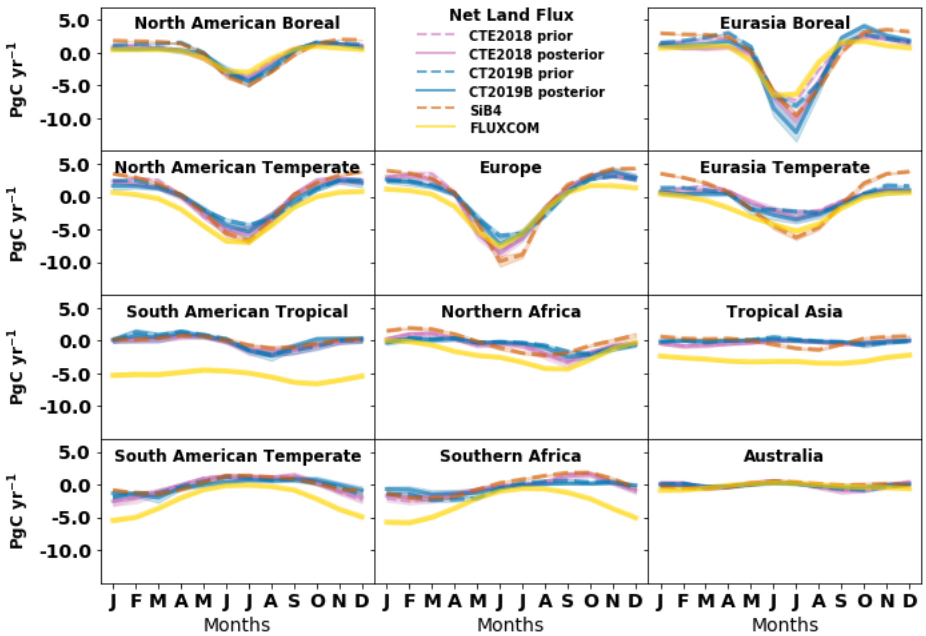


**Figure 2. Monthly averaged NEE of $CO_2$ for terrestrial TransCom regions between 2000 and 2017. Positive values indicate a flux from the biosphere to the atmosphere, and the shaded regions represent the 1-σ standard deviation of each model's monthly fluxes.**

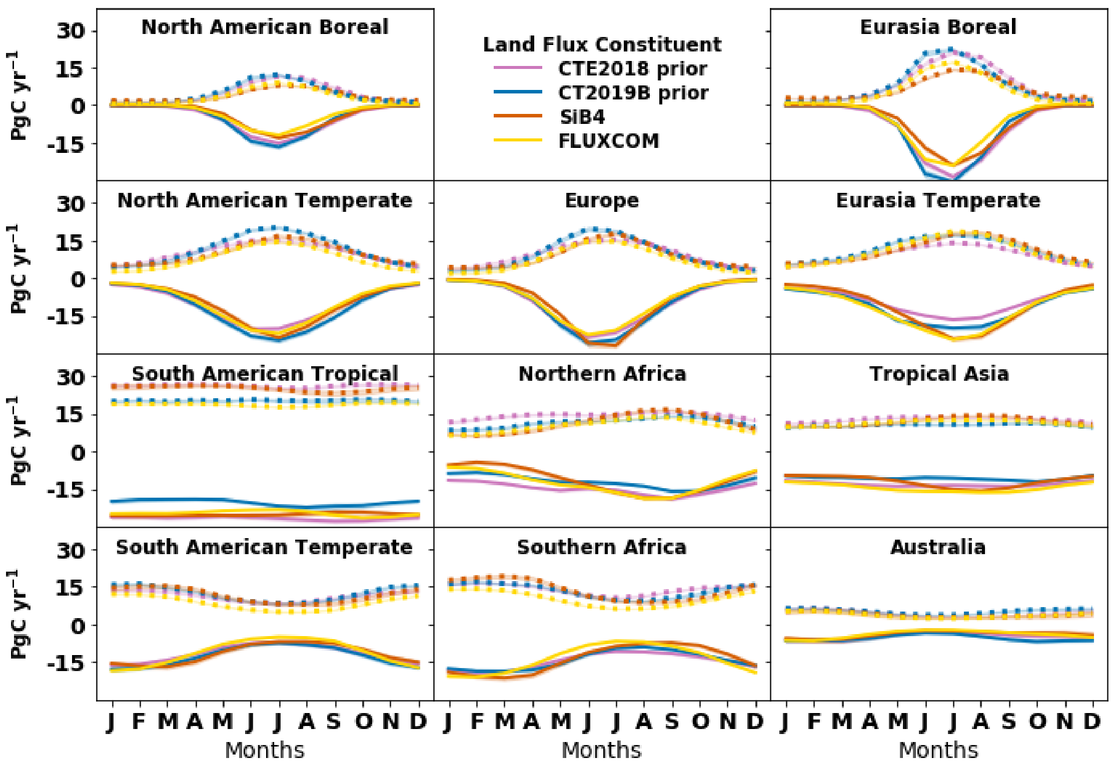


**Figure 3. Monthly averaged gross primary production (GPP, solid lines) and ecosystem respiration (RE, dotted lines) for terrestrial TransCom regions between the years 2000 and 2017. Positive values indicate a flux from the biosphere to the atmosphere, and the shaded regions represent the 1-σ standard deviation of each model's monthly fluxes.**

Monthly NEE, GPP, and RE seasonal cycles are compared across “top-down” and “bottom-up” models. In general, we find all models agree more in the Northern Hemisphere regions than Southern Hemisphere regions or the tropical regions (Figure 2 and Figure S1). This agreement between “multiple constraint” approaches may result from the greater density of observations in the Northern Hemisphere, leading to more information about surface fluxes.

In the Northern Hemisphere boreal regions, modeled NEE seasonal cycles disagree mostly on the strength of Eurasian boreal carbon uptake in the summer months and carbon release in the dormant months. July NEE rates vary by as much as 6.0 PgC among the models, with FLUXCOM showing the least uptake and CT2019B having the most uptake. In the summer months, small differences in NEE between models mask large differences between the component fluxes GPP and RE (Figure 3). For example, FLUXCOM, SiB4, and the CTE2018 prior (SiBCASA) have similar NEE summertime uptake in the Eurasia boreal region (an averaged difference between models of 2.9 PgC yr-1), but the amplitude in GPP and RE vary greatly among the models (an averaged difference of 7.3 and 7.1 PgC yr-1 respectively). Similarly, for Boreal North American, the seasonal amplitude of the modeled NEE agrees better (an averaged difference between models of 1.4 PgC yr-1), compared to their respective GPP and RE seasonal amplitudes (an averaged difference of 4.3 and 4.2 PgC yr-1 respectively).

In Northern Hemisphere temperate regions, NEE among models agrees better for North America and Europe than for Eurasia (see Figure S1). For the Eurasian temperate region, FLUXCOM and SiB4 have a stronger summertime uptake (both by ~3 PgC $yr^{-1}$) than both the CarbonTracker priors and posteriors. In the winter, FLUXCOM and CarbonTracker priors and posteriors show similar near-zero NEE whereas SiB4 shows net outgassing of up to 3.6 PgC $yr^{-1}$. Here, SiB4 has a stronger NEE seasonal amplitude rate than other models that is driven mainly by its strong GPP seasonality. These specific regions have an abundance of deciduous trees and it is possible SiB4 overestimates deciduous seasonality.

For Tropical South America, there is good agreement in NEE seasonality between SiB4, both CarbonTracker posteriors, and their respective prior estimates (ranges from $r^2$=0.85 to 0.99 between comparison combinations). By contrast, FLUXCOM NEE seasonality does not agree well with other models (ranging from $r^2$=0.09 to 0.32) and shows peak carbon uptake in October whereas other models show a peak in August. FLUXCOM shows a stronger net carbon uptake (by ~6 PgC $yr^{-1}$) than all other models throughout the year (see Figure S2 and S3). This strong carbon sink is driven mainly by a weaker RE (by as much as 8.0 PgC $yr^{-1}$) whereas it's GPP strength is within the variability of other models.

For the Northern and Southern African regions and South American Temperate region, FLUXCOM shows a stronger seasonality than other models. Particularly in the Northern and Southern African regions, FLUXCOM shows stronger NEE uptake (ranging from 4.1 to 5.2 PgC $yr^{-1}$) than other models from December to February.

For Australia, the averaged NEE seasonality amplitude difference between models is 0.3 PgC yr-1. Both CarbonTracker priors (i.e. CASA-GFED and SiBCASA) show a NEE minimum in September to October that is not captured by FLUXCOM or SiB4. Across the southern hemisphere regions, both CTE2018 prior and posterior NEE seasonal cycles are nearly identical ($r^2$=0.99 to

1.0), whereas CT2019B posterior seasonality shows more seasonal variability than its prior counterpart (CASA-GFED) with a correlation between $r^2$=0.7 to 0.87.

### 3.2 Annual Total Emissions Analysis

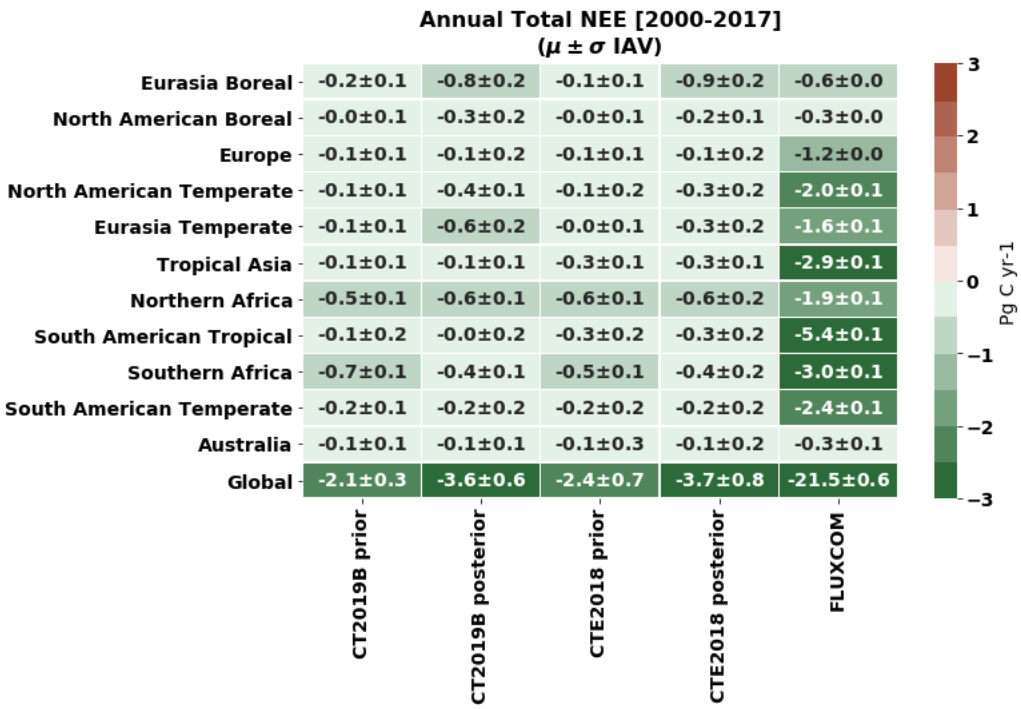


**Figure 4. Annual mean and 1-sigma interannual variability (IAV) of net ecosystem exchange (NEE) for each TransCom region from 2000-2017. Negative values (in green) indicate a carbon uptake from the atmosphere into the biosphere. TransCom regions are arranged top-to-bottom to align with relative latitudinal locations with global estimates at the bottom.**

In our annual total NEE analysis, we find both CarbonTracker posteriors and priors, and FLUXCOM agree that each TransCom region is a net carbon sink (Figure 4). SiB4 is not included in this analysis as it assumes a long-term carbon balance. CT2019B and CTE2018 posterior NEE estimate global annual uptake is -3.6±0.6 and -3.7±0.8 PgC $yr^{-1}$, respectively. These estimates agree within each model's interannual variability (IAV) and suggest stronger carbon uptake than their prior counterparts by up to 2.1 and 1.3 PgC $yr^{-1}$. Both CT2019B and CTE2018 posterior NEE suggest more carbon uptake than their priors (CASA-GFED and SiBCASA respectively) in the boreal regions (an annual difference of 0.6 to 0.8 PgC $yr^{-1}$, respectively) and also to a lesser extent in the temperate Eurasian and North American regions (a difference of 0.2 to 0.3 PgC $yr^{-1}$). By contrast, posterior NEE shows less carbon uptake than prior estimates in the Southern African region (a difference of 0.1 to 0.3 PgC $yr^{-1}$). CarbonTracker posteriors suggest the largest carbon sinks are found in Eurasian and African regions, whereas their prior estimates suggest only African regions. FLUXCOM NEE shows stronger carbon uptake than other models in all regions except at northern boreal latitudes. FLUXCOM estimates global annual carbon uptake to be -21.5±0.6 PgC $yr^{-1}$.

### 3.3 Trend Analysis

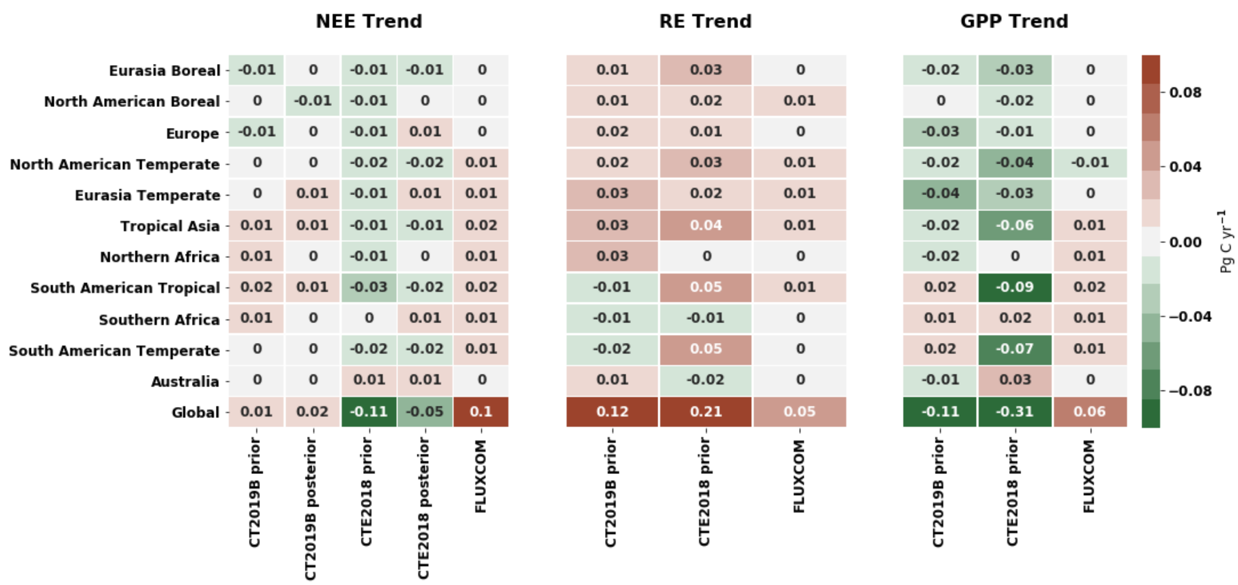


**Figure 5. Trends of annual total NEE, RE, and GPP for different TransCom regions estimated for 2000-2017. Negative values (more green) represent an increase in carbon uptake, and positive values (more brown) represent an increase in carbon release.**

Using a linear regression of each model's terrestrial fluxes over an 18-year period, we determine whether the global carbon cycle has changed as estimated by different modeling techniques and observational constraints (e.g. atmospheric observations, flux measurements and NDVI-derived GPP). We find both inversions show more net carbon release in time than the NDVI-based models used as prior estimates by both inversions (Figure 5). The CT2019B prior shows an increase in both GPP and RE over time, with RE slightly stronger by 0.01 PgC $yr^{-1}$ resulting in a small net carbon release over time. The CTE2018 SiBCASA prior also shows an increase in both GPP and RE over time, yet with a slightly stronger GPP resulting in net carbon uptake. By contrast, FLUXCOM shows a small global decrease in net carbon uptake by 0.1 PgC $yr^{-1}$. However, no model's NEE trends are found to be statistically "meaningful" according to the criterion (i.e. $r^2 \geq 0.65$ at $p \leq 0.05$) defined by Bryhn & Dimbeg, (2011).

### 3.3 Seasonal Amplitude Change Analysis

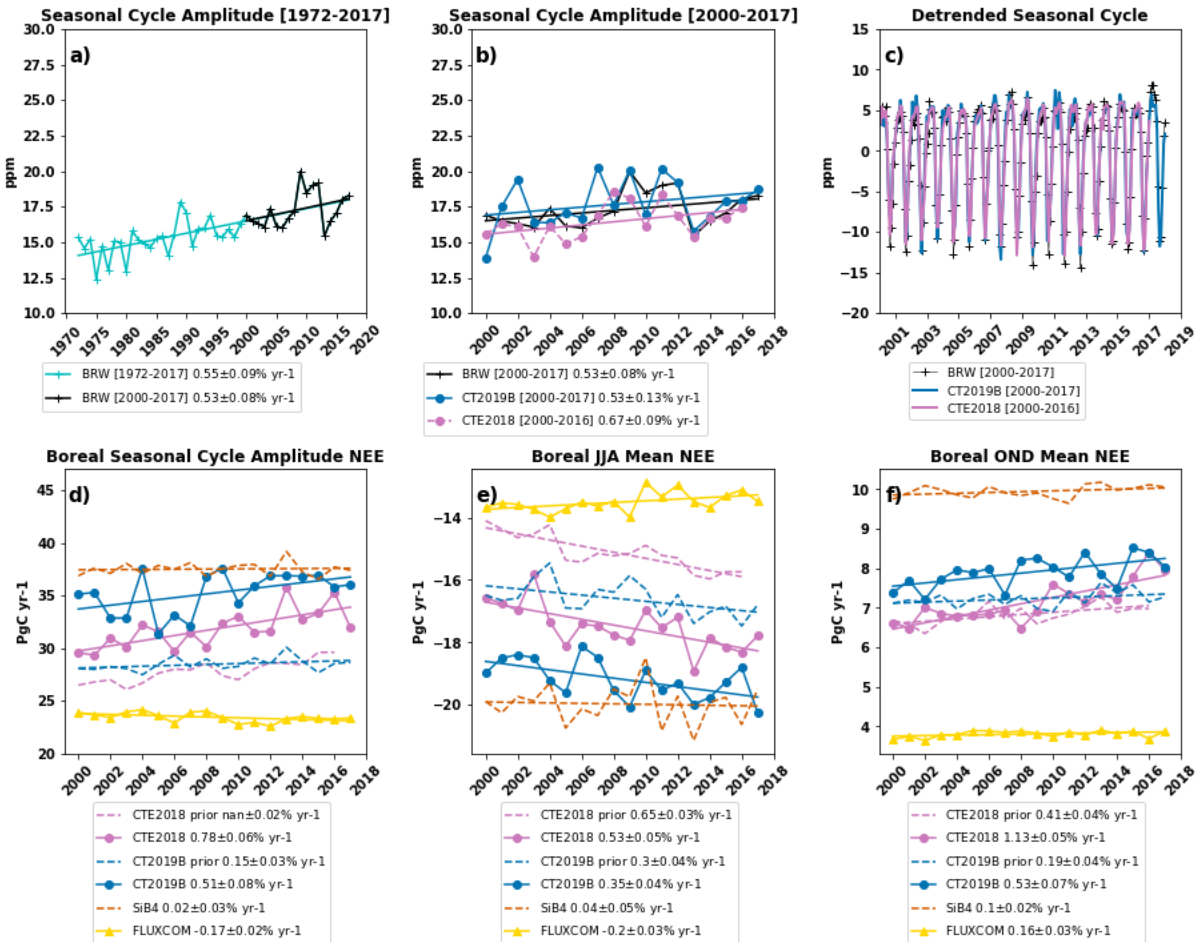


**Figure 6. (a) $CO_2$ seasonal amplitudes (in ppm) and trends (% $yr^{-1}$) observed at BRW observatory from 1972-2017 and 2000-2017; (b) "zoomed-in" $CO_2$ seasonal amplitude and trend from BRW from 2000-2017 with estimates from CT2019B and CTE2018 posteriors; (c) the $CO_2$ seasonal cycle at BRW with estimates from CT2019B and CTE2018 posteriors; (d) annual boreal region (i.e., north of 45°N) peak-to-trough NEE amplitudes in units of PgC $yr^{-1}$ from both CarbonTracker posteriors and priors, FLUXCOM, and SiB4; (e) boreal region NEE annually averaged over the peak productivity months of June, July, and August (JJA); and**

**(f) boreal region NEE annually averaged over the early winter months of October, November, and December (OND).**

We calculated the average annual growth rate of the $CO_2$ seasonal amplitude at BRW over the full current record 1972-2017 and compared it with Graven et al. (2013). We find the $CO_2$ peak-to-trough amplitude trend over full record at BRW to be 0.55±0.09%$yr^{-1}$, which is within the standard deviation of the 0.60%$yr^{-1}$ trend estimated by Graven et al., (2013) from 1961-2011 (Figure 6a). Over the time period considered in our study, 2000-2017, we estimate the observed seasonal amplitude growth rate to be 0.53±0.08%$yr^{-1}$, within a standard deviation of the 1972-2011 growth rate.

We also find that both CT2019B and CTE2018 simulated $CO_2$ mole fractions have nearly identical seasonal cycles at BRW from 2000-2017 (with an agreement of $r^2$=0.99). Atmospheric inversions are also able to capture the observed seasonal cycle amplitude trend at BRW from 2000-2017. Here, CT2019B simulated $CO_2$ mole fractions show a trend of 0.53±0.13%$yr^{-1}$, nearly exactly the same as what is observed, whereas CTE2018 suggests a stronger trend of 0.67±0.09%$yr^{-1}$ but within 1-sigma standard deviation of BRW observations (Figure 6a-c).

Because both inversions were able to reproduce the $CO_2$ seasonal amplitude trend at BRW, we use them to examine the source of this increased $CO_2$ seasonal amplitude using NEE fluxes. We note that it is expected that inversions are able to reproduce the observations because they are constrained by these observations at BRW and other sites, although biased priors could prevent inversions from reproducing the annual cycle amplitude trend. Using the high latitude band (north of 45˚N) criteria as considered in Graven et al. (2013), CT2019B shows a NEE amplitude trend of 0.38±0.09%$yr^{-1}$ and CTE2018 shows a NEE amplitude trend of 0.78±0.06%$yr^{-1}$ (Figure 6d). Both inversions' NEE amplitude trends are within 1-sigma standard deviation of their $CO_2$ seasonal amplitude trends.

At high latitudes, the boreal seasonal amplitude of NEE for both CarbonTracker posterior estimates significantly exceed their priors by between 0.17 and 0.23%$yr^{-1}$. The CarbonTracker posteriors also have larger boreal seasonal amplitudes than FLUXCOM (by between 0.55 and 0.95%$yr^{-1}$) and SiB4 (by between 0.36 and 0.76%$yr^{-1}$). Whereas CarbonTracker priors have a positive trend in seasonal amplitude, SiB4 does not have any trend and FLUXCOM shows a small negative trend.

We consider that the NEE amplitude trends at high boreal latitude could mainly be attributed to increased uptake during months of highest productivity (June, July, and August (JJA)) or increased emission by soil respiration early in the cold season (October, November, and December (OND)). We observe that, in absolute values, CTE2018's early winter mean NEE trend ($1.13\pm0.05\%yr^{-1}$) is nearly double that of its summertime NEE trend ($-0.53\pm0.05\%yr^{-1}$), whereas both CT2019B's early winter ($0.39\pm0.08\%yr^{-1}$) and summer NEE trends ($-0.3\pm0.04\%yr^{-1}$) are within error bars of each other over the 18-year period (see Figure 6e-f). Compared to the NDVI constrained models used as priors for both inversions, posterior estimates for both inversions show a weaker net carbon uptake in the summertime and a greater carbon release in early winter. In early winter, both posteriors mean NEE trends exceed the variability of their prior counterparts. In summer, only the CTE2018 NEE trend exceeds the variability of its prior.

Inversions cannot directly tell us whether a trend of seasonally averaged NEE is a result of a change in carbon uptake or respiration because these are not estimated individually, but the NDVI constrained models provide some insight. In the summer months, both CarbonTracker posterior and prior estimates show a negative NEE trend which implies more net carbon uptake. Here, both SiBCASA and CASA-GFED show a greater growth rate in GPP than RE (Figure S4). By contrast, in the early winter, both CarbonTracker posterior and prior estimates show a positive NEE trend which implies more net carbon release. CTE2018 prior shows a greater growth rate of RE than GPP. CT2019B prior shows a decrease in GPP as well as an increase in RE.

At high latitudes, SiB4 NEE amplitude is larger than other models, but does not show a change in NEE amplitude over the past two decades ($-0.02\pm0.03\%yr^{-1}$). However, it shows small increases in net carbon uptake in summertime ($-0.04\pm0.05\%yr^{-1}$) and net release in early winter ($0.10\pm0.02\%yr^{-1}$). These NEE growth rates are a result of increased growth in both boreal GPP and RE in both summer and early winter months, and are dependent on each of the flux's initial flux strength in year 2000. By contrast to both inversions and other TBMs over the 18-year period, FLUXCOM shows a positive NEE trend, meaning more carbon efflux, in the summer months ($0.2\pm0.03\%yr^{-1}$) in addition to positive NEE trend in the summer months ($0.16\pm0.03\%yr^{-1}$). We note that we also examined other seasons and at different latitudinal bands and did not find any large changes in NEE between models.

# 4 Discussion

## 4.1 Terrestrial carbon flux seasonality and annual rates

We compared atmospheric inversions, prognostic and diagnostic TBMs, and bottom-up terrestrial carbon flux products to gain insights about the carbon cycle in terms of terrestrial carbon flux seasonality and annual biospheric emissions.

In the northern hemisphere boreal regions, both inversions show an annual carbon sink (between -0.7 and -0.9 PgC $yr^{-1}$) that is stronger than their prior estimates (between -0.1 and -0.2 PgC $yr^{-1}$). This difference is mainly due to increased carbon uptake in the summer months in the inversions and indicates atmospheric $CO_2$ measurements call for a stronger carbon sink than their prior flux fields that rely on satellite-based NDVI data. NDVI and other satellite driven light-use efficiency models often failed to capture seasonal photosynthetic dynamics at northern latitudes such as seasonal photosynthetic activity of boreal evergreen forests (Gamon et al., 1995; 2016). Though FLUXCOM and the inversions show similar seasonal cycles and annual NEE rates for northern boreal regions, these results may be fortuitous because of the large temporal and spatial gaps in both $CO_2$ measurements and FLUXNET data as well as their different scaling methods that incorporate these limited observations. Issues with upscaling site-level FLUXNET data include how different ecosystem heterogeneity such as plant function types and environmental drivers such as atmospheric conditions change at different scales (Tramontana et al., 2016). In addition to temporospatial gaps in the atmospheric $CO_2$ observational network, errors in top-down estimates depend on accurately quantifying the uncertainties of the prior fluxes in the data assimilation scheme and the accuracy in atmospheric transport used to link observed atmospheric $CO_2$ to surface carbon fluxes. Uncertainties in atmospheric transport can propagate systematic errors in both the global annual carbon budget and the magnitude of seasonal cycle around the world (Schuh et al., 2019). Both CarbonTracker priors suggest the northern boreal regions have experienced more carbon uptake (of up to -0.03 $PgCyr^{-1}$) and more carbon release (of up to 0.03 $PgCyr^{-1}$) over the past 18-years that has resulted in a small net terrestrial carbon sink (of up to -0.01 $PgCyr^{-1}$). However, these trends at high boreal regions, as well as across all other regions, are not significantly meaningful. This insignificance may result from no important changes in biogenic carbon sources or sinks have occurred over this time period. Another possible explanation is there are not enough observations to reduce the current noise. With more observations in these regions over a longer time period, we will likely be able to detect important changes in terrestrial carbon sources and sinks.

In the northern temperate regions including Europe, CT2019B and CTE2018 posterior flux estimates are similar to prior estimates for Europe, but posteriors show greater uptake relative to priors in the North American and Eurasian temperate region. In Europe, where there is a relative abundance of available atmospheric $CO_2$ observations compared to other temperate latitudes, similarities between priors and posteriors may imply CarbonTracker priors are pretty close to the true value for Europe. In other regions, posteriors show more carbon uptake than their priors. This may suggest priors underestimate carbon uptake at temperate regions, but there may be other possibilities. It may be true that fossil fuel assumptions prescribed in the CarbonTracker DA scheme are incorrect. A recent study by Basu et al. (2020) reported that many U.S. fossil fuel $CO_2$ emission inventories, including the US Environmental Protection Agency (EPA), may be significantly underestimated. This study conducted an independent emission monitoring evaluation over North America using atmospheric inversions constrained by both atmospheric $CO_2$ and $\Delta^{14}CO_2$ measurements collected as part of NOAA's Global Greenhouse Gas Reference Network. If fossil fuel emissions are under-estimated in the CarbonTracker DA scheme (which does not revise prior estimates of fossil fuel emissions), this may result in an underestimation of natural carbon sinks or overestimation of sources. For the temperate regions that account for the most fossil fuel emissions, biased fossil fuel $CO_2$ emissions likely will cause potential biases in posterior NEE rates. Another possibility for differences between CT2019B and CTE2018 NEE fluxes at temperate regions is the different set of observations used in the assimilation process. For example, CT2019B has recently assimilated the extensive Siberian tower measurements collected by the National Institute for Environmental Studies.

For tropical regions, we find that posterior fluxes match prior flux estimates, and that FLUXCOM has a significantly stronger carbon sink throughout the year. In the South American Tropical region, CTE2018's seasonal cycle and annual uptake is nearly identical ($r^2$=0.99) to its prior estimate, whereas CT2019B shows more seasonal variability ($r^2$=0.85) and a stronger annual uptake rate (by 0.2 $PgCyr^{-1}$). A close resemblance of posteriors to their priors, as shown by CTE2018, typically indicates limited observational coverage in these regions. CT2019B's increased variability and an increase in uptake rates could be the result of assimilating aircraft data across Brazil collected by the Instituto de Pesquisas Energéticas e Nucleares (IPEN).

Likewise, for Tropical Asia, CTE2018's seasonal variability and annual uptakes (-0.1 $PgCyr^{-1}$) are little unchanged from prior estimates. CT2019B has the same uptake rates as it's prior estimate, but shows greater seasonal variability ($r^2$=0.79). This greater seasonal variability could be related to assimilated shipboard observations across the Pacific Ocean collected by the National Institute for Environmental Studies (NIES).

FLUXCOM shows a stronger uptake rate during all months, by up to 2.6 $PgCyr^{-1}$ in Tropical Asia, and 5.1 $PgCyr^{-1}$ in the South American Tropics. FLUXCOM also has a different seasonal cycle from the inversions, NDVI-constrained models, and SiB4 ($r^2$=0.09 to 0.32). A possible explanation for this may be our choice of FLUXCOM ensemble product. We chose the ensemble median of 6 members with ERA-5 meteorological forcing data setups that included all three machine learning methods and both flux partitioning methods. However, Jung et al. (2020) state that the large tropical carbon sink in FLUXCOM is consistent among all the FLUXCOM setups and ensemble members. A possible explanation for this large carbon sink may be systematic biases in observational GPP or RE. However, recent studies (Campioli et al., 2016; Spielmann et al., 2019) have reported no systematic biases in FLUXNET GPP used in upscaled global FLUXCOM GPP. Tropical carbon loss fluxes by fire, land-use change, or evasion from inland waters are reportedly missing from FLUXNET observations but likely only offset half the tropical carbon sink (Zscheischler et al., 2017). Another possible explanation for FLUXCOM's large tropical sink includes upscaling issues. Upscaling sparse ground-based site-level flux observations over a large region with heterogeneous vegetation and varying meteorological conditions can be a challenge (Fu et al., 2019).

## 4.2 Changes in boreal Seasonal Amplitude

We combine CarbonTracker inversions, remote-sensing TBMs, and the prognostic TBM SiB4 to determine possible causes of the $CO_2$ seasonal amplitude increase at BRW over the past two decades. CarbonTracker inversions capture the observed $CO_2$ seasonal amplitude trend at BRW from 2000-2017 and their $CO_2$ seasonal amplitudes are within 1-sigma standard deviation of their northern boreal (45-90˚N) NEE amplitude trends. This implies a link between the $CO_2$ seasonal amplitude trend and the northern boreal NEE amplitude trend. CarbonTracker priors and posteriors suggests that the NEE amplitude trends are a response to both increased rates of carbon uptake in the summer months and increased carbon release in the early winter months.

Top-down and bottom-up estimates confirm various remote-sensing and atmospheric $CO_2$ observational studies that have reported heterogenous greening and browning trends at northern high latitudes. These trends are linked to enhanced biomass cover and productivity (Pan et al., 2011; Myers-Smith et al., 2020; Xu et al., 2013; Wenzel et al., 2016; Forkal et al., 2016) driven by arctic warming (Elmendorf et al., 2012; Zhu et al., 2016). The same Arctic warming has also resulted in enhanced by carbon release due to microbial decomposition in soil driven (Commane et al., 2014; Natali et al., 2019). We find CarbonTracker models to have a greater NEE amplitude growth rate than the bottom-up estimates. This greater growth rate is a result of enhanced early-winter carbon release. This finding agrees with evidence for large early-winter respiration flux in the northern boreal latitudes that offsets carbon uptake in summer months. Commane et al. (2014) combined aircraft and tower $CO_2$, eddy covariance flux data, and satellite remote sensing to estimate the Alaskan carbon budget from 2012-2014 and found that the seasonal amplitude of $CO_2$ in early winter is likely due to carbon release from soil organic matter. Natali et al. (2019) synthesized in-situ carbon flux data over the arctic using machine learning methods to show winter carbon release due to microbial decomposition in soil is stronger than carbon uptake during the growing season.

Another possible explanation for why top-down estimates show a greater NEE amplitude trend than bottom-up estimates is that bottom-up TBMs rely on satellite-based NDVI and light-use efficiency models which have been shown to inadequately capture seasonal photosynthetic activity at northern latitudes such as seasonal photosynthetic activity of boreal evergreen forests (Gamon et al., 1995; 2016). However, top-down posterior estimates show a slower rate of change in NEE during summer months than their respective priors. Some studies have used TBMs to suggest the increase is associated with mid-latitude agriculture intensification across North America (Zeng et al., 2014; Gray et al., 2014). A more recent study used a top-down approach to suggest Siberian and temperate ecosystems are mainly responsible (Lin et al., 2020).

The current configuration of SiB4 does not simulate the effects of increasing $CO_2$ or land-use change and therefore is not expected to produce a long-term net sink or source of carbon. It is however expected to show a response to inter-annual climate variability. This is likely why we see only a negligible change to the boreal seasonal amplitude of NEE, but see an increase in summertime carbon uptake and early-winter carbon respiration with variability. Such changes in boreal carbon productivity and respiration rates are often linked with woody vegetation expansion and warmer temperatures in the arctic. However, SiB4 does not simulate changes in land cover types over time, so the greater GPP and RE in SiB4 may be directly associated with warmer temperatures. As SiB4 begins to incorporate additional carbon sources and sinks that offset its annual carbon balance (e.g. disturbances, dynamic vegetation, $CO_2$ fertilization, nutrient limitation, and regrowth), this TBM may prove instrumental in testing the impact of these factor in regional to global carbon budget analysis.

Jung et al., 2020 reports northern cold regions are poorly represented by FLUXNET sites which likely cause extrapolation issues used in the upscaling process. This makes sense that limited observations cause challenges in upscaling carbon fluxes over a large region with vast heterogeneous vegetation. In order to adequately capture changes and variability of carbon fluxes in northern boreal ecosystems, more observations are needed. Though northern boreal ecosystems are shown to have smaller NEE interannual variability than other ecological regions (Baldocchi et al., 2018), FLUXCOM has underestimated interannual variability compared to inversions (Jung et al., 2020). The reason is unclear, but underestimated variability may be caused by machine-learning methods chosen by FLUXCOM (Tramontana et al., 2016; Marcolla et al., 2017). Representing changes in the boreal region NEE requires accounting for variations in soil moisture, water balance. Resolving changes in NEE variability in boreal ecosystems requires continuous measurements of environmental factors such as soil moisture, water balance, and air temperature (Baldocchi et al., 2018). Increasing the size of the FLUXNET network, improving its machine-learning methods, and resolving environmental factors will improve the quality of the FLUXCOM product.

## 5 Conclusions

We combined advanced data-driven and process-based modeling techniques to provide insight into present-day terrestrial carbon cycle processes and how they may be changing in response to climate variability and trends. We find that models typically agree in terms of seasonal variability, and all show an annual carbon sink for all regions across the globe. Models presented in this study imply that the net global annual carbon sink has not changed significantly between the years 2000 and 2017. We learned that the CarbonTracker system captures the observed increase in the seasonal amplitude of $CO_2$ at BRW, and suggests that this growth may have less to do with increased productivity in summer months than increased carbon outgassing rates during early winter months. Such increased boreal carbon outgassing rates are also found from bottom-up estimates from FLUXCOM. The combination of process-based and "multiple constraint" models present an opportunity to understand how the carbon cycle processes respond to climate change.

**Acknowledgments:**

This research was sponsored by NOAA Climate Program Office, Atmospheric Chemistry, Carbon Cycle and Climate. Datasets for this research are included in this paper (and it's supplementary information files): CarbonTracker Europe posterior and prior results are provided by Wageningen University in collaboration with the ObsPack partners (http://www.carbontracker.eu). CarbonTracker CT2019B posterior and prior results are provided by NOAA ESRL, Boulder, Colorado, USA from the website at http://carbontracker.noaa.gov. SiB4 is available online https://gitlab.com/kdhaynes/sib4_corral).

## References

Anav, A., Friedlingstein, P., Kidston, M., Bopp, L., Ciais, P., Cox, P., … Zhu, Z. (2013). Evaluating the Land and Ocean Components of the Global Carbon Cycle in the CMIP5 Earth System Models. Journal of Climate, 26(18), 6801–6843. https://doi.org/10.1175/JCLI-D-12-00417.1

Baker, I. T., Harper, A. B., da Rocha, H. R., Denning, A. S., Araújo, A. C., Borma, L. S., … Wofsy, S. C. (2013). Surface ecophysiological behavior across vegetation and moisture gradients in tropical South America. Agricultural and Forest Meteorology, 182–183, 177–188. https://doi.org/10.1016/j.agrformet.2012.11.015

Baker, I. T., Prihodko, L., Denning, A. S., Goulden, M., Miller, S., & Rocha, H. R. da. (2008). Seasonal drought stress in the Amazon: Reconciling models and observations. Journal of Geophysical Research: Biogeosciences, 113(G1). https://doi.org/10.1029/2007JG000644

Baldocchi, D., Chu, H., & Reichstein, M. (2018). Inter-annual variability of net and gross ecosystem carbon fluxes: A review. Agricultural and Forest Meteorology, 249, 520–533. https://doi.org/10.1016/j.agrformet.2017.05.015

Basu, S., Lehman, S. J., Miller, J. B., Andrews, A. E., Sweeney, C., Gurney, K. R., Xu, X., Southon, J., & Tans, P. P. (2020). Estimating US fossil fuel CO2 emissions from measurements of 14C in atmospheric CO2. Proceedings of the National Academy of Sciences, 117(24), 13300–13307. https://doi.org/10.1073/pnas.1919032117

Berrisford P., Kållberg P., Kobayashi S., Dee D., Uppala S., Simmons A. J., … Sato H. (2011). Atmospheric conservation properties in ERA-Interim. Quarterly Journal of the Royal Meteorological Society, 137(659), 1381–1399. https://doi.org/10.1002/qj.864

Campioli, M., Malhi, Y., Vicca, S., Luyssaert, S., Papale, D., Peñuelas, J., Reichstein, M., Migliavacca, M., Arain, M. A., & Janssens, I. A. (2016). Evaluating the convergence between eddy-covariance and biometric methods for assessing carbon budgets of forests. Nature Communications, 7(1), 13717. https://doi.org/10.1038/ncomms13717

Carbontracker Team; (2018) : Compilation of near real time atmospheric carbon dioxide data; obspack_co2_1_NRT_v4.2_2018-04-06; NOAA Earth System Research Laboratory, Global Monitoring Division. http://doi.org/10.15138/G3RP8K.

Collatz, G. J., Ribas-Carbo, M., & Berry, J. A. (1992). Coupled Photosynthesis-Stomatal Conductance Model for Leaves of C4 Plants. Functional Plant Biology, 19(5), 519–538. https://doi.org/10.1071/pp9920519

Collatz, G. James, Ball, J. T., Grivet, C., & Berry, J. A. (1991). Physiological and environmental regulation of stomatal conductance, photosynthesis and transpiration: A model that includes a laminar boundary layer. Agricultural and Forest Meteorology, 54(2), 107–136. https://doi.org/10.1016/0168-1923(91)90002-8

Conway, T. J., Tans, P. P., Waterman, L. S., Thoning, K. W., Kitzis, D. R., Masarie, K. A., & Zhang, N. (1994). Evidence for interannual variability of the carbon cycle from the National Oceanic and Atmospheric Administration/Climate Monitoring and Diagnostics Laboratory Global Air Sampling Network. Journal of Geophysical Research: Atmospheres, 99(D11), 22831–22855. https://doi.org/10.1029/94JD01951

Cooperative Global Atmospheric Data Integration Project; (2017): Multi-laboratory compilation of atmospheric carbon dioxide data for the period 1957-2016; obspack_co2_1_GLOBALVIEWplus_v3.2_2017_11_02; NOAA Earth System Research Laboratory, Global Monitoring Division. http://dx.doi.org/10.15138/G3704H'

Cooperative Global Atmospheric Data Integration Project. (2019). Multi-laboratory compilation of atmospheric carbon dioxide data for the period 1957-2018; obspack_co2_1_GLOBALVIEWplus_v5.0_2019_08_12 (Data set). NOAA Earth System Research Laboratory, Global Monitoring Division. https://doi.org/10.25925/20190812

Commane, R., Lindaas, J., Benmergui, J., Luus, K. A., Chang, R. Y.-W., Daube, B. C., Euskirchen, E. S., Henderson, J. M., Karion, A., Miller, J. B., Miller, S. M., Parazoo, N. C., Randerson, J. T., Sweeney, C., Tans, P., Thoning, K., Veraverbeke, S., Miller, C. E., & Wofsy, S. C. (2017). Carbon dioxide sources from Alaska driven by increasing early winter respiration from Arctic tundra. Proceedings of the National Academy of Sciences, 114(21), 5361–5366. https://doi.org/10.1073/pnas.1618567114

Copernicus Climate Change Service (C3S) (2017): ERA5: Fifth generation of ECMWF atmospheric reanalyses of the global climate . Copernicus Climate Change Service Climate Data Store (CDS), date of access. https://cds.climate.copernicus.eu/cdsapp#!/home

Cox, P. M., Pearson, D., Booth, B. B., Friedlingstein, P., Huntingford, C., Jones, C. D., & Luke, C. M. (2013). Sensitivity of tropical carbon to climate change constrained by carbon dioxide variability. Nature, 494(7437), 341–344. https://doi.org/10.1038/nature11882

Dee, D. P., Uppala, S. M., Simmons, A. J., Berrisford, P., Poli, P., Kobayashi, S., … Vitart, F. (2011). The ERA-Interim reanalysis: Configuration and performance of the data assimilation system. Quarterly Journal of the Royal Meteorological Society, 137(656), 553–597. https://doi.org/10.1002/qj.828

Delworth, T. L., Broccoli, A. J., Rosati, A., Stouffer, R. J., Balaji, V., Beesley, J. A., … Zhang, R. (2006). GFDL's CM2 Global Coupled Climate Models. Part I: Formulation and Simulation Characteristics. Journal of Climate, 19(5), 643–674. https://doi.org/10.1175/JCLI3629.1

Farquhar, G. D., von Caemmerer, S., & Berry, J. A. (1980). A biochemical model of photosynthetic CO2 assimilation in leaves of C 3 species. Planta, 149(1), 78–90. https://doi.org/10.1007/BF00386231

Flato, G., J. Marotzke, B. Abiodun, P. Braconnot, S.C. Chou, W. Collins, P. Cox, F. Driouech, S. Emori, V. Eyring, C. Forest, P. Gleckler, E. Guilyardi, C. Jakob, V. Kattsov, C. Reason and M. Rummukainen, 2013: Evaluation of Climate Models. In: Climate Change 2013: The Physical Science Basis. Contribution of Working Group I to the Fifth Assessment Report of the Intergovernmental Panel on Climate Change (Stocker, T.F., D. Qin, G.-K. Plattner, M. Tignor, S.K. Allen, J. Boschung, A. Nauels, Y. Xia, V. Bex and P.M. Midgley (eds.)). Cambridge University Press, Cambridge, United Kingdom and New York, NY, USA.

Friedlingstein, P., Cox, P., Betts, R., Bopp, L., von Bloh, W., Brovkin, V., … Zeng, N. (2006). Climate-Carbon Cycle Feedback Analysis: Results from the C4MIP Model Intercomparison. Journal of Climate, 19(14), 3337–3353. https://doi.org/10.1175/JCLI3800.1

Friedlingstein, Pierre, Meinshausen, M., Arora, V. K., Jones, C. D., Anav, A., Liddicoat, S. K., & Knutti, R. (2013). Uncertainties in CMIP5 Climate Projections due to Carbon Cycle Feedbacks. Journal of Climate, 27(2), 511–526. https://doi.org/10.1175/JCLI-D-12-00579.1

Forkel, M., Carvalhais, N., Rödenbeck, C., Keeling, R., Heimann, M., Thonicke, K., Zaehle, S., & Reichstein, M. (2016). Enhanced seasonal CO2 exchange caused by amplified plant productivity in northern ecosystems. Science, 351(6274), 696–699. https://doi.org/10.1126/science.aac4971

Fu, Z., Gerken, T., Bromley, G., Araújo, A., Bonal, D., Burban, B., Ficklin, D., Fuentes, J. D., Goulden, M., Hirano, T., Kosugi, Y., Liddell, M., Nicolini, G., Niu, S., Roupsard, O., Stefani, P., Mi, C., Tofte, Z., Xiao, J., … Stoy, P. C. (2018). The surface-atmosphere exchange of carbon dioxide in tropical rainforests: Sensitivity to environmental drivers and flux measurement methodology. Agricultural and Forest Meteorology, 263, 292–307. https://doi.org/10.1016/j.agrformet.2018.09.001

Gamon, J. A., Field, C. B., Goulden, M. L., Griffin, K. L., Hartley, A. E., Joel, G., Peñuelas, J., & Valentini, R. (1995). Relationships Between NDVI, Canopy Structure, and Photosynthesis in Three Californian Vegetation Types. Ecological Applications, 5(1), 28–41. JSTOR. https://doi.org/10.2307/1942049

Gamon, J. A., Huemmrich, K. F., Wong, C. Y. S., Ensminger, I., Garrity, S., Hollinger, D. Y., Noormets, A., & Peñuelas, J. (2016). A remotely sensed pigment index reveals photosynthetic phenology in evergreen conifers. Proceedings of the National Academy of Sciences, 113(46), 13087–13092. https://doi.org/10.1073/pnas.1606162113

Gurney, K. R., Law, R. M., Denning, A. S., Rayner, P. J., Pak, B. C., Baker, D., … Taguchi, S. (2004). Transcom 3 inversion intercomparison: Model mean results for the estimation of seasonal carbon sources and sinks. Global Biogeochemical Cycles, 18(1). https://doi.org/10.1029/2003GB002111

Hawkins, E., & Sutton, R. (2009). The Potential to Narrow Uncertainty in Regional Climate Predictions. Bulletin of the American Meteorological Society, 90(8), 1095–1108. https://doi.org/10.1175/2009BAMS2607.1

Haynes, K., Baker, I. T., Denning, S., Stöckli, R., Schaefer, K., Lokupitiya, E. Y., & Haynes, J. M. ( 2019a). Representing grasslands using dynamic prognostic phenology based on biological growth stages: 1. Implementation in the Simple Biosphere Model (SiB4). Journal of Advances in Modeling Earth Systems, 11, 4423– 4439. https://doi.org/10.1029/2018MS001540

Haynes, K. D., Baker, I. T., Denning, A. S., Wolf, S., Wohlfahrt, G., Kiely, G., et al. ( 2019b). Representing grasslands using dynamic prognostic phenology based on biological growth stages: 2. Carbon cycling. Journal of Advances in Modeling Earth Systems, 11, 4440– 4465. https://doi.org/10.1029/2018MS001541

Hofmann, D. J., Butler, J. H., Dlugokencky, E. J., Elkins, J. W., Masarie, K., Montzka, S. A., & Tans, P. (2006). The role of carbon dioxide in climate forcing from 1979 to 2004: Introduction of the Annual Greenhouse Gas Index. Tellus B, 58(5), 614–619. https://doi.org/10.1111/j.1600-0889.2006.00201.x

Jacobson, A. R., Fletcher, S. E. M., Gruber, N., Sarmiento, J. L., & Gloor, M. (2007). A joint atmosphere-ocean inversion for surface fluxes of carbon dioxide: 1. Methods and global-scale fluxes. Global Biogeochemical Cycles, 21(1). https://doi.org/10.1029/2005GB002556

A. R. Jacobson, K. N. Schuldt, J. B. Miller, T. Oda, P. Tans, A. Andrews, J. Mund, L. Ott, G. J. Collatz,T. Aalto, S. Afshar, K. Aikin, S. Aoki, F. Apadula, B. Baier, P. Bergamaschi, A. Beyersdorf, S. C. Biraud,A. Bollenbacher, D. Bowling, G. Brailsford, J. B. Abshire, G. Chen, H. Chen, L. Chmura, Sites Climadat,A. Colomb, S. Conil, A. Cox, P. Cristofanelli, E. Cuevas, R. Curcoll, C. D. Sloop, K. Davis, S. D. Wekker,M. Delmotte, J. P. DiGangi, E. Dlugokencky, J. Ehleringer, J. W. Elkins, L. Emmenegger, M. L. Fischer,G. Forster, A. Frumau, M. Galkowski, L. V. Gatti, E. Gloor, T. Griffis, S. Hammer, L. Haszpra, J. Hatakka,M. Heliasz, A. Hensen, O. Hermanssen, E. Hintsa, J. Holst, D. Jaffe, A. Karion, S. R. Kawa, R. Keeling,P. Keronen, P. Kolari, K. Kominkova, E. Kort, P. Krummel, D. Kubistin, C. Labuschagne, R. Langenfelds,O. Laurent, T. Laurila, T. Lauvaux, B. Law, J. Lee, I. Lehner, M. Leuenberger, I. Levin, J. Levula, J. Lin,M. Lindauer, Z. Loh, M. Lopez, C. Lund Myhre, T. Machida, I. Mammarella, G. Manca, A. Manning, A.Manning, M. V. Marek, P. Marklund, M. Y. Martin, H. Matsueda, K. McKain, H. Meijer, F. Meinhardt, N.Miles, C. E. Miller, M. Molder, S. Montzka, F. Moore, J.-A. Morgui, S. Morimoto, B. Munger, J. Necki, S. ¨Newman, S. Nichol, Y. Niwa, S. ODoherty, M. Ottosson-Lofvenius, B. Paplawsky, J. Peischl, O. Peltola, J.-¨M. Pichon, S. Piper, C. Plass-Dolmer, M. Ramonet, E. Reyes-Sanchez, S. Richardson,

H. Riris, T. Ryerson, ¨K. Saito, M. Sargent, M. Sasakawa, Y. Sawa, D. Say, B. Scheeren, M. Schmidt, A. Schmidt, M. Schumacher, P. Shepson,M. Shook, K. Stanley, M. Steinbacher, B. Stephens, C. Sweeney, K. Thoning, M. Torn, J. Turnbull, K.Tørseth, P. V. D. Bulk, I. T. V. D. Laan-Luijkx, D. V. Dinther, A. Vermeulen, B. Viner, G. Vitkova, S.Walker, D. Weyrauch, S. Wofsy, D. Worthy, D. Young, and M. Zimnoch. CarbonTracker CT2019B, 2020.DOI: 10.25925/39m3-6069

Jung, M., Reichstein, M., Schwalm, C. R., Huntingford, C., Sitch, S., Ahlström, A., … Zeng, N. (2017). Compensatory water effects link yearly global land $CO_2$ sink changes to temperature. Nature, 541(7638), 516–520. https://doi.org/10.1038/nature20780

Kaushik, A., J. Graham, K. Dorheim, R. Kramer, J. Wang, and B. Byrne (2020), The future of the carbon cycle in a changing climate, Eos, 101, https://doi.org/10.1029/2020EO140276. Published on 20 February 2020.

Krol, M., Houweling, S., Bregman, B., Broek, M. van den, Segers, A., Velthoven, P. van, … Bergamaschi, P. (2005). The two-way nested global chemistry-transport zoom model TM5: Algorithm and applications. Atmospheric Chemistry and Physics, 5(2), 417–432. https://doi.org/10.5194/acp-5-417-2005

Lokupitiya, E., Denning, S., Paustian, K., Baker, I., Schaefer, K., Verma, S., … Fischer, M. (2009). Incorporation of crop phenology in Simple Biosphere Model (SiBcrop) to improve land-atmosphere carbon exchanges from croplands. Biogeosciences, 6(6), 969–986. https://doi.org/10.5194/bg-6-969-2009

Mao, J., Ribes, A., Yan, B., Shi, X., Thornton, P. E., Séférian, R., Ciais, P., Myneni, R. B., Douville, H., Piao, S., Zhu, Z., Dickinson, R. E., Dai, Y., Ricciuto, D. M., Jin, M., Hoffman, F. M., Wang, B., Huang, M., & Lian, X. (2016). Human-induced greening of the northern extratropical land surface. Nature Climate Change, 6(10), 959–963. https://doi.org/10.1038/nclimate3056

Marcolla, B., Rödenbeck, C., & Cescatti, A. (2017). Patterns and controls of inter-annual variability in the terrestrial carbon budget. Biogeosciences, 14(16), 3815–3829. https://doi.org/10.5194/bg-14-3815-2017

Masarie, K. A., Peters, W., Jacobson, A. R., & Tans, P. P. (2014). ObsPack: A framework for the preparation, delivery, and attribution of atmospheric greenhouse gas measurements. Earth System Science Data, 6(2), 375–384. https://doi.org/10.5194/essd-6-375-2014

Meehl, G., Stocker, T., Collins, W. D., Friedlingstein, P., Gaye, A. T., Gregory, J. M., … Zhao, Z.-C. (2007). Global climate projections climate change 2007: The physical science basis. The Physical Science Basis, 747–845.

Milly, P. C. D., Malyshev, S. L., Shevliakova, E., Dunne, K. A., Findell, K. L., Gleeson, T., … Swenson, S. (2014). An Enhanced Model of Land Water and Energy for Global Hydrologic and Earth-System Studies. Journal of Hydrometeorology, 15(5), 1739–1761. https://doi.org/10.1175/JHM-D-13-0162.1

Mu, M., Randerson, J. T., Werf, G. R. van der, Giglio, L., Kasibhatla, P., Morton, D., … Wennberg, P. O. (2011). Daily and 3-hourly variability in global fire emissions and consequences for atmospheric model predictions of carbon monoxide. Journal of Geophysical Research: Atmospheres, 116(D24). https://doi.org/10.1029/2011JD016245

Natali, S. M., Watts, J. D., Rogers, B. M., Potter, S., Ludwig, S. M., Selbmann, A.-K., Sullivan, P. F., Abbott, B. W., Arndt, K. A., Birch, L., Björkman, M. P., Bloom, A. A., Celis, G., Christensen, T. R., Christiansen, C. T., Commane, R., Cooper, E. J., Crill, P., Czimczik, C., … Zona, D. (2019). Large loss of CO 2 in winter observed across the northern permafrost region. Nature Climate Change, 9(11), 852–857. https://doi.org/10.1038/s41558-019-0592-8

Oda, T., & Maksyutov, S. (2011). A very high-resolution (1 km×1 km) global fossil fuel $CO_2$ emission inventory derived using a point source database and satellite observations of nighttime lights. Atmospheric Chemistry and Physics, 11(2), 543–556. https://doi.org/10.5194/acp-11-543-2011

Olsen, S. C., & Randerson, J. T. (2004). Differences between surface and column atmospheric CO2 and implications for carbon cycle research. Journal of Geophysical Research: Atmospheres, 109(D2). https://doi.org/10.1029/2003JD003968

Pan, Y., Birdsey, R. A., Fang, J., Houghton, R., Kauppi, P. E., Kurz, W. A., Phillips, O. L., Shvidenko, A., Lewis, S. L., Canadell, J. G., Ciais, P., Jackson, R. B., Pacala, S. W., McGuire, A. D., Piao, S., Rautiainen, A., Sitch, S., & Hayes, D. (2011). A Large and Persistent Carbon Sink in the World's Forests. Science, 333(6045), 988–993. https://doi.org/10.1126/science.1201609

Parazoo, N. C., Magney, T., Norton, A., Raczka, B., Bacour, C., Maignan, F., Baker, I., Zhang, Y., Qiu, B., Shi, M., MacBean, N., Bowling, D. R., Burns, S. P., Blanken, P. D., Stutz, J., Grossmann, K., & Frankenberg, C. (2020). Wide discrepancies in the magnitude and direction of modeled solar-induced chlorophyll fluorescence in response to light conditions. Biogeosciences, 17(13), 3733–3755. https://doi.org/10.5194/bg-17-3733-2020

Peters, W., Jacobson, A. R., Sweeney, C., Andrews, A. E., Conway, T. J., Masarie, K., … Tans, P. P. (2007). An atmospheric perspective on North American carbon dioxide exchange: CarbonTracker. Proceedings of the National Academy of Sciences, 104(48), 18925–18930. https://doi.org/10.1073/pnas.0708986104

Potter, C. S., Randerson, J. T., Field, C. B., Matson, P. A., Vitousek, P. M., Mooney, H. A., & Klooster, S. A. (1993). Terrestrial ecosystem production: A process model based on global satellite and surface data. Global Biogeochemical Cycles, 7(4), 811–841. https://doi.org/10.1029/93GB02725

Project, C. G. A. D. I. (2017). Multi-laboratory compilation of atmospheric carbon dioxide data for the period 1957-2016; obspack_co2_1_GLOBALVIEWplus_v3.1_2017-10-18 (Data set). https://doi.org/10.15138/g3t055

Quéré, C. L., Raupach, M. R., Canadell, J. G., Marland, G., Bopp, L., Ciais, P., … Woodward, F. I. (2009). Trends in the sources and sinks of carbon dioxide. Nature Geoscience, 2(12), 831–836. https://doi.org/10.1038/ngeo689

Quéré, C. Le, Moriarty, R., Andrew, R. M., Canadell, J. G., Sitch, S., Korsbakken, J. I., … Zeng, N. (2015). Global Carbon Budget 2015. Earth System Science Data, 7(2), 349–396. https://doi.org/10.5194/essd-7-349-2015

Quéré, Corinne Le, Andrew, R. M., Friedlingstein, P., Sitch, S., Pongratz, J., Manning, A. C., … Zhu, D. (2018). Global Carbon Budget 2017. Earth System Science Data, 10(1), 405–448. https://doi.org/10.5194/essd-10-405-2018

Randerson, J. T., Van Der Werf, G. R., Giglio, L., Collatz, G. J., & Kasibhatla, P. S. (2015). Global Fire Emissions Database, Version 4.1 (GFEDv4). ORNL DAAC. https://doi.org/10.3334/ORNLDAAC/1293

Randerson, James T., Thompson, M. V., Malmstrom, C. M., Field, C. B., & Fung, I. Y. (1996). Substrate limitations for heterotrophs: Implications for models that estimate the seasonal cycle of atmospheric CO2. Global Biogeochemical Cycles, 10(4), 585–602. https://doi.org/10.1029/96GB01981

Schaefer, K., Collatz, G. J., Tans, P., Denning, A. S., Baker, I., Berry, J., … Philpott, A. (2008). Combined Simple Biosphere/Carnegie-Ames-Stanford Approach terrestrial carbon cycle model. Journal of Geophysical Research: Biogeosciences, 113(G3), G03034. https://doi.org/10.1029/2007JG000603

Schuh, A. E., Jacobson, A. R., Basu, S., Weir, B., Baker, D., Bowman, K., … Palmer, P. I. (2019). Quantifying the Impact of Atmospheric Transport Uncertainty on CO2 Surface Flux Estimates. Global Biogeochemical Cycles, 33(4), 484–500. https://doi.org/10.1029/2018GB006086

Sellers, P. j., Randall, D. a., Collatz, G. j., Berry, J. a., Field, C. b., Dazlich, D. a., … Bounoua, L. (1996). A Revised Land Surface Parameterization (SiB2) for Atmospheric GCMS. Part I: Model Formulation. Journal of Climate, 9(4), 676–705. https://doi.org/10.1175/1520-0442(1996)009<0676:ARLSPF>2.0.CO;2

Smith, D. C. (2019). Using remotely sensed fluorescence and soil moisture to better understand the seasonal cycle of tropical grasslands (Thesis, Colorado State University. Libraries). Retrieved from https://mountainscholar.org/handle/10217/185785

Spielmann, F. M., Wohlfahrt, G., Hammerle, A., Kitz, F., Migliavacca, M., Alberti, G., Ibrom, A., El-Madany, T. S., Gerdel, K., Moreno, G., Kolle, O., Karl, T., Peressotti, A., & Vedove, G. D. (2019). Gross Primary Productivity of Four European Ecosystems Constrained by Joint CO2 and COS Flux Measurements. Geophysical Research Letters, 46(10), 5284–5293. https://doi.org/10.1029/2019GL082006

Stephens, B. B., Gurney, K. R., Tans, P. P., Sweeney, C., Peters, W., Bruhwiler, L., … Denning, A. S. (2007). Weak northern and strong tropical land carbon uptake from vertical profiles of atmospheric CO2. Science (New York, N.Y.), 316(5832), 1732–1735. https://doi.org/10.1126/science.1137004

Taylor, K. E., Stouffer, R. J., & Meehl, G. A. (2012). An Overview of CMIP5 and the Experiment Design. Bulletin of the American Meteorological Society, 93(4), 485–498. https://doi.org/10.1175/BAMS-D-11-00094.1

Tramontana, G., Jung, M., Schwalm, C. R., Ichii, K., Camps-Valls, G., Ráduly, B., … Papale, D. (2016). Predicting carbon dioxide and energy fluxes across global FLUXNET sites with regression algorithms. Biogeosciences, 13(14), 4291–4313. https://doi.org/10.5194/bg-13-4291-2016

Tucker, C. J. (1979). Red and photographic infrared linear combinations for monitoring vegetation. Remote Sensing of Environment, 8(2), 127–150. https://doi.org/10.1016/0034-4257(79)90013-0

van der Laan-Luijkx, I. T., van der Velde, I. R., van der Veen, E., Tsuruta, A., Stanislawska, K., Babenhauserheide, A., … Peters, W. (2017). The CarbonTracker Data

Assimilation Shell (CTDAS) v1.0: Implementation and global carbon balance 2001–2015. Geosci. Model Dev., 10(7), 2785–2800. https://doi.org/10.5194/gmd-10-2785-2017

van der Werf, G. R., Randerson, J. T., Giglio, L., Leeuwen, T. T. van, Chen, Y., Rogers, B. M., … Kasibhatla, P. S. (2017). Global fire emissions estimates during 1997–2016. Earth System Science Data, 9(2), 697–720. https://doi.org/10.5194/essd-9-697-2017

van der Werf, G. R. V. D., Randerson, J. T., Collatz, G. J., & Giglio, L. (2003). Carbon emissions from fires in tropical and subtropical ecosystems. Global Change Biology, 9(4), 547–562. https://doi.org/10.1046/j.1365-2486.2003.00604.x

Wenzel, S., Cox, P. M., Eyring, V., & Friedlingstein, P. (2016). Projected land photosynthesis constrained by changes in the seasonal cycle of atmospheric CO2. Nature, 538(7626), 499–501. https://doi.org/10.1038/nature19772

Zscheischler, J., Mahecha, M. D., Avitabile, V., Calle, L., Carvalhais, N., Ciais, P., Gans, F., Gruber, N., Hartmann, J., Herold, M., Ichii, K., Jung, M., Landschützer, P., Laruelle, G. G., Lauerwald, R., Papale, D., Peylin, P., Poulter, B., Ray, D., … Reichstein, M. (2017). Reviews and syntheses: An empirical spatiotemporal description of the global surface-atmosphere carbon fluxes: opportunities and data limitations. Biogeosciences, 14(15), 3685–3703. https://doi.org/10.5194/bg-14-3685-2017

**Supplemental Materials**

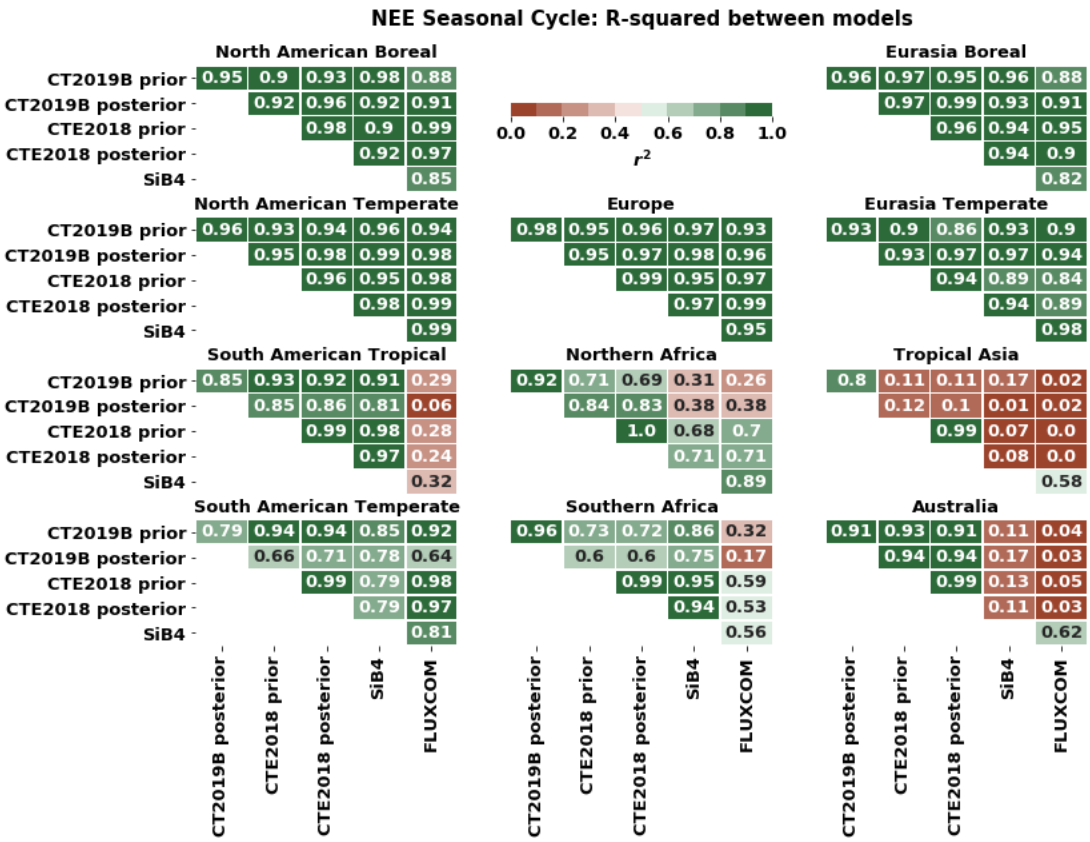


**Figure S1.** Coefficient of determination, or r-squared, values between model's monthly averaged net ecosystem exchange (NEE) at TransCom regions between 2000 and 2017. Green colors represent good model agreement and red represents poor agreement.

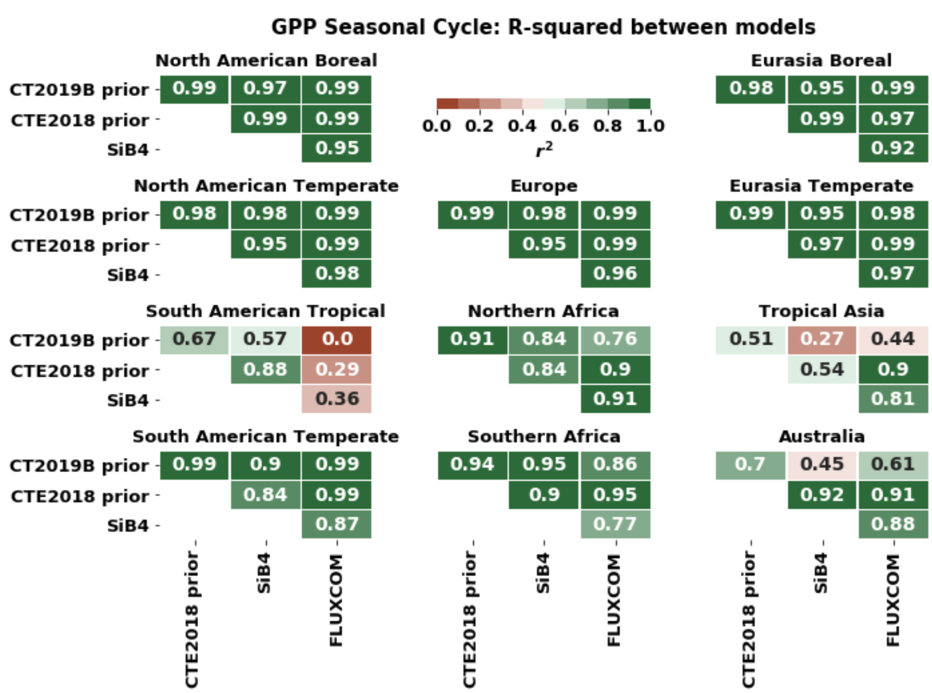

**Figure S2.** Coefficient of determination, or r-squared, values between model's monthly averaged gross primary production (GPP) at TransCom regions between 2000 and 2017. Green colors represent good model agreement and red represents poor agreement.

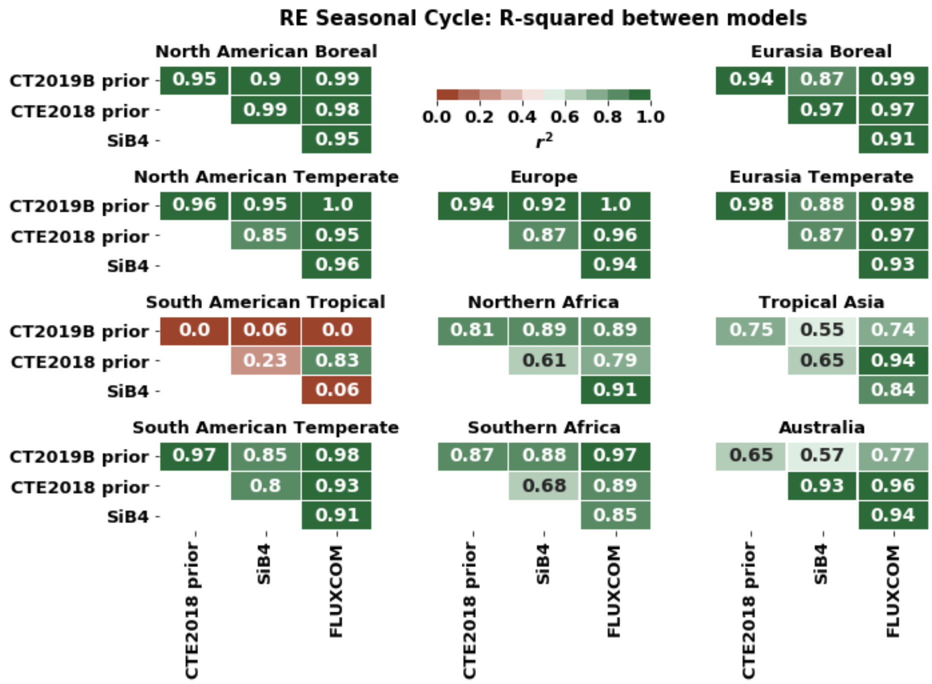


**Figure S3.** Coefficient of determination, or r-squared, values between model's monthly averaged ecosystem respiration (RE) at TransCom regions between 2000 and 2017. Green colors represent good model agreement and red represents poor agreement.

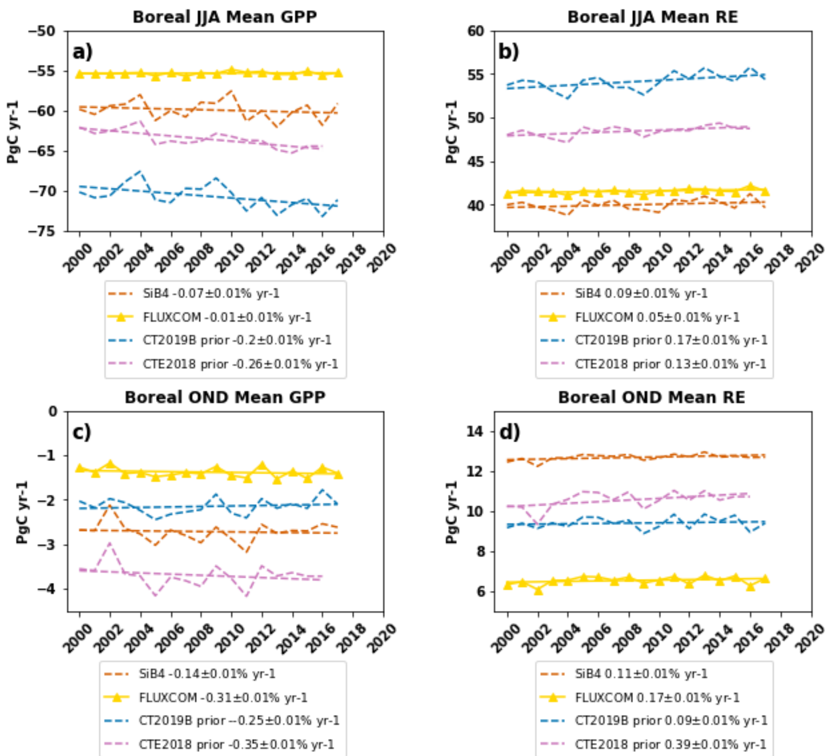


**Figure S4. (a) Boreal region (i.e. north of 45˚N) seasonal amplitudes of GPP in the summer months of June, July, and August (JJA) for CarbonTracker priors, FLUXCOM, and SiB4; (b) as well as the seasonal amplitudes of RE; and (c) boreal region seasonal amplitudes of GPP in the early winter months of October, November, and December (OND) (d) as well as the seasonal amplitudes of RE.**